Extended Hückel theory for band structure, chemistry, and transport. I. Carbon nanotubes

D. Kienle[a)]
Department of Electrical and Computer Engineering, Purdue University, West Lafayette, Indiana 47907

J. I. Cerda
Instituto de Ciencia de Materiales de Madrid, CSIC, Cantoblanco, 28049 Madrid, Spain

A. W. Ghosh
Department of Electrical and Computer Engineering, University of Virginia, Charlottesville, Virginia 22903

(Received 6 January 2006; accepted 21 June 2006; published online 29 August 2006)

We describe a semiempirical atomic basis extended Hückel theoretical (EHT) technique that can be used to calculate bulk band structure, surface density of states, electronic transmission, and interfacial chemistry of various materials within the same computational platform. We apply this method to study multiple technologically important systems, starting with carbon nanotubes and their interfaces and silicon-based heterostructures in our follow-up paper [D. Kienle *et al.*, J. Appl. Phys. **100**, 043715 (2006), following paper]. We find that when it comes to quantum transport through interesting, complex heterostructures including gas molecules adsorbed on nanotubes, the Hückel band structure offers a fair and practical compromise between orthogonal tight-binding theories with limited transferability between environments under large distortion and density functional theories that are computationally quite expensive for the same purpose. © *2006 American Institute of Physics*. [DOI: 10.1063/1.2259818]

I. INTRODUCTION

Quantitative electronic structure theories are essential to the understanding and design of materials and devices. It is now generally accepted that transport properties of nanoscale devices depend on both the intrinsic electronic structure of the active channel, as well as its interfacial properties with contacts and other scattering centers. A particular challenge in this respect is to incorporate both long and short range correlations within the same framework, such as the bulk band structure of periodic solids as well as the local chemical properties of clusters, surfaces, and interfaces. For instance, simulating scanning tunneling spectra (STS) of molecules on silicon substrates requires an accurate description of the silicon bulk band structure that quantitatively captures not just the band gap responsible for the onset of negative differential resistance[1] but also the multiple effective masses which determine the contact density of states and injection velocities and the strain parametrizations that capture atomic reconstruction and relaxation near the surface and their bonding with molecular components.[2] In addition, one needs to describe the electrostatics responsible for band bending in the silicon depletion layer, the molecular transport levels and their transmission under bias, and finally the electronic properties of the scanning tip and the intervening vacuum layer, all within the same formalism. It is no surprise therefore that under these circumstances, standard electronic structure techniques developed by quantum chemists for simulating molecules are usually incompatible with those developed by solid-state physicists for bulk band structure, making it important to develop a common formalism that addresses both domains of interest and also maintains a good compromise between computational accuracy and practicality.

While sophisticated methods exist for equilibrium geometry and band structure, comparable success has yet to be achieved for transport problems, partly because of the lack of universally accepted experimental standards, but mainly because quantum transport inherently involves solving a complicated nonequilibrium open boundary problem for which electronic structure theories are not benchmarked. A proper quantitative understanding of correlation effects in transport is still evolving and it is not yet clear if mean-field approaches that work at equilibrium are at all capable of handling the profusion of electronic excitations that often dominate in nanoscale conduction.[3,4] Even aside from such correlation issues, one needs to worry about heterointerfaces, since current flow involves charge transport across two intrinsically different material systems—a multimoded contact consisting of a highly conductive material externally maintained at thermal equilibrium and a sparsely moded device region that is readily driven away from equilibrium and acts as the active transport channel.

In this paper, we employ a semiempirical approach to electronic structure that can be adopted for electronic conduction through complex hybrid systems by combining it with the nonequilibrium Green's function (NEGF) technique for quantum transport. Our theoretical parameters are tailored to salient features of the bulk band structure, while the employment of nonorthogonal basis sets resembling linear combinations of underlying atomic orbitals seems to make them fairly transferable to surfaces as well, as observed in the past.[5,6] In addition, the presence of explicit basis sets

[a)]Electronic mail: kienle@ecn.purdue.edu

opens up the possibility of "stitching" together disparate regions[7] by matching the interfacial Green's function, which is the *only* quantity through which the diverse regions communicate with each other quantum mechanically. The modularity of our approach also allows us to conveniently separate the problems of determining the optimized interfacial geometry and the interfacial transmission (we are ignoring current-induced forces), the former depending on the total energy of the system while the latter depends only on a few relevant single-electron levels near the Fermi energy. In other words, given a particular atomistic configuration of the contact-channel-contact heterostructure, we seek to determine its transport properties *by coupling our electronic structure approach with quantum transport using NEGF.*

The outline of the paper is as follows. Section II explains the strengths of extended Hückel theory (EHT) over other traditional band structure methods. In Sec. III we briefly summarize the NEGF approach used to calculate density of states and transmission of CNTs; we then specify the model Hamiltonian and describe the details of EHT used to determine the band structure. The numerically calculated band structure data for nanotubes are then compared in Sec. IV with experimental scanning tunneling spectroscopy experiments along with other theoretical approaches. In Sec. V we investigate the changes in the dispersion of a semiconducting carbon nanotube (CNT) under large lateral deformations as well as with a CO molecular attachment to its surface that allows it to function as a molecular sensor. We summarize our work and discuss future extensions in the last section.

II. WHY THIS PARTICULAR METHOD?

A particular trade-off in any band structure theory is between flexibility and rigor. While empirical, orthogonal tight-binding (OTB) methods are quick and practical, they are benchmarked for specific geometries and are usually not very transferable to other environments involving significant structural deformations beyond a few percent. Tight-binding basis sets are commonly assumed to be both orthogonal and short ranged,[5] while atomic wave functions are not, meaning that OTB basis sets do not resemble eigenstates of an atomic Hamiltonian. Efforts at improving tight-binding theories involve going beyond nearest-neighbor techniques, using higher virtual orbital bases for increased completeness[8–10] and employing power laws for parameter transfer under small ($\sim 1\% - 2\%$) strain.[11] Nevertheless these models are likely to miss important chemical details involving properties varying on an interatomic length scale, in particular, near deformed surfaces and interfaces where a drastic reconstruction of the atomic structure is expected.[5]

At the other end of the spectrum are accurate, but computationally expensive, first-principles techniques developed by quantum chemists and solid-state physicists, such as configuration interaction (CI) and density functional theories (DFTs) in various atomic or plane wave basis sets or combinations thereof. Structural deformations are naturally captured by such total energy calculations by solving a one electron Schrödinger equation in a suitable self-consistent potential approximating the electron-electron interaction.[12–14] Such codes are typically based on rigorous variational theorems and are quantitatively quite accurate, at least for equilibrium properties. Their extension and practical implementation to transport beyond the linear response regime are continuously evolving[15–17] and a topic of current research.[18] Conceptually, it is not clear if any self-consistent potential approach can quantitatively describe the rich spectrum of many-body transitions that are often experimentally accessed in strongly correlated transport in weakly coupled systems.[3,4]

We aim for a practical compromise between these two limits by using a semiempirical technique motivated by extended Hückel calculations popular in the chemistry community. Such theories, widely used in the past to describe the equilibrium properties of isolated molecules,[19] have recently been applied to molecular conduction[20] and also extended to solids using transferable atomic-orbital (AO) basis sets for calculating the electronic structure of various compounds benchmarked with detailed DFT calculations within the local density approximation (LDA) or generalized gradient (GGA) approximation.[21] Given a geometry, one uses the explicit EHT basis functions to calculate a nonorthogonal overlap matrix S, which along with separately fitted onsite Hamiltonian matrix elements yields the corresponding off-diagonal hopping elements of the Hamiltonian. Within the standard Hückel prescription, structural changes are simply accounted for by recalculating the overlap and hopping elements but leaving the basis sets and onsite elements unchanged.

In the following, we apply this EHT parametrization scheme[21] by benchmarking it to a two-dimensional graphene sheet[22,23] and extending it to obtain the band structure, density of states, and electronic transmission of carbon nanotubes (CNTs) of varying chiralities. We show that the same bulk-optimized EHT parameters (onsite energies and AO-basis functions) are transferable to small diameter CNT band structures, capturing even curvature-induced band gap effects for larger than 1%–3% tube deformation, in quantitative agreement with STS data. Furthermore, surface chemical effects are examined through the study of nanotube based carbon monoxide sensors whose alteration of electronic structure upon molecular adsorption compares favorably with *ab initio* calculations of da Silva *et al.*[24] In our follow-up paper,[25] we will demonstrate a similar transferability between bulk silicon and various silicon surfaces and apply the EHT methodology to unreconstructed silicon nanowires. Taken together, the wide variety of these examples illustrates the range of transferability of EHT parameters, which we believe makes extended Hückel theory a useful practical tool for electronic structure and quantum transport.

III. APPROACH

Simulating conduction through a heterostructure involves combining suitable band structures for the channel and contact materials with self-consistent electrostatics and quantum transport. While the formulation of correlated transport is itself an active area of research, our aim here is to develop a minimal model that would capture quantum chemistry, surface physics, band structure, and electrostatic effects

that are all crucial for different prominent aspects of nanoscale conduction. The ingredients needed for a proper simulation are the Hamiltonian and potential matrices describing the device band structure and electrostatics and the contact self-energies that effectively open up the system and allow us to add or remove charge under nonequilibrium conditions. The EHT prescription gives us a practical way to calculate these ingredient matrices for a given atomistic structure and then connect them with a nonequilibrium Green's function (NEGF) formulation of quantum transport, which we briefly summarize below.[26,27] The retarded Green's function of the device is given by

$$G = [(E + i\eta)S - H - \Sigma_l - \Sigma_r]^{-1}, \tag{1}$$

where S and H describe the overlap and Hamiltonian matrices of the device unit cell calculated according to the Hückel prescription Eq. (5). The matrix elements $\Sigma_{l,r}$ are self-energies that provide open boundary conditions to the device with the left and right semi-infinite contacts. The self-energy $\Sigma = \tau g \tau^\dagger$ incorporates the coupling matrix τ describing the contact-device bonding, while g is the surface Green's function of the left/right contact calculated by means of a recursion technique.[28,29] In a nonorthogonal tight-binding scheme, the density of states (DOS) is given by $D(E) = (i/2\pi)\mathrm{Tr}(AS)$, where $A = i(G - G^\dagger)$ denotes the spectral function. Finally, in the phase-coherent limit, the zero-bias transmission through the unit cell reads $T(E) = \mathrm{Tr}[\Gamma_l G \Gamma_r G^\dagger]$, where $\Gamma_{l,r} = i(\Sigma_{l,r} - \Sigma_{l,r}^\dagger)$ are the broadening matrices which specify the time an electron resides within the device. In this paper, we will study infinite nanotubes so that the active device is just one CNT unit cell and the left and right contacts extend that cell to infinity in either direction.

The band structure of a nanotube with chirality (n,m) is calculated employing the nonorthogonal Slater-Koster scheme and solving for the generalized eigenvalue problem[30]

$$\mathbf{H}(\mathbf{k})A_i(\mathbf{k}) = E_i(\mathbf{k})\mathbf{S}(\mathbf{k})A_i(\mathbf{k}), \tag{2}$$

where $A_i(\mathbf{k})$ denotes the eigenvector of the ith subband and $\mathbf{k}$ is a Bloch wave vector within the first Brillouin zone. The size of the overlap and Hamiltonian matrices are determined by the chosen basis set, i.e., the number of atoms within the unit cell multiplied by the number of orbitals per atom. In our case, using four sp orbitals per atom, the size of these matrices is 80×80 for an armchair (5,5) tube as sketched in Fig. 1. The overlap and Hamilton matrices, $\mathbf{S}(\mathbf{k})$ and $\mathbf{H}(\mathbf{k})$, representing the structure in reciprocal space are calculated by

$$\mathbf{H}_{i,j}(\mathbf{k}) = \sum_{j',m'} e^{i\mathbf{k}\cdot(\mathbf{R}_{i0} - \mathbf{R}_{j'm'})}\mathbf{H}_{i0,j'm'}, \tag{3}$$

$$\mathbf{S}_{i,j}(\mathbf{k}) = \sum_{j',m'} e^{i\mathbf{k}\cdot(\mathbf{R}_{i0} - \mathbf{R}_{j'm'})}\mathbf{S}_{i0,j'm'}, \tag{4}$$

where i and j label atoms within the unit cell and m' is the unit cell index. The summation indices in $\mathbf{H}_{i,j}(\mathbf{k})$ and $\mathbf{S}_{i,j}(\mathbf{k})$ run over all atoms j' in unit cell m' which are equivalent to atom j in the reference unit cell $m=0$. The real-space matrix elements $\mathbf{H}_{i0,j'm'}$ and $\mathbf{S}_{i0,j'm'}$ between an atom i in the reference unit cell and atom j' in cell m' are calculated by means of the extended Hückel prescription.

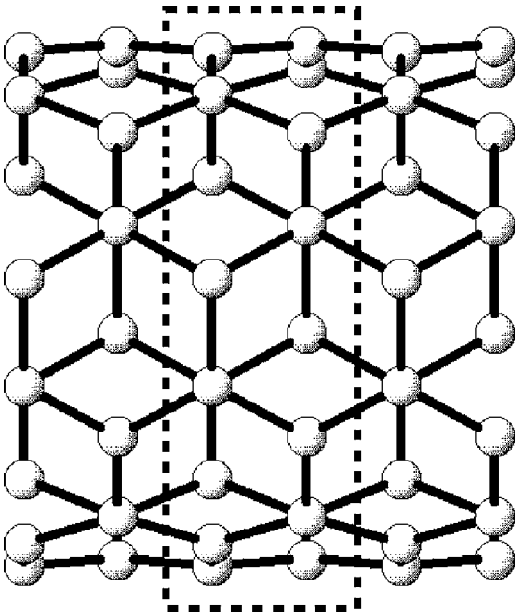

FIG. 1. Sketch of a (5, 5) armchair tube with three unit cells. The dashed rectangle marks the center unit cell containing 20 carbon atoms. For the calculation of the E-k dispersion we use the first nearest-neighbor unit cells to the left and right, respectively.

Perhaps the most prominent difference between the empirical tight-binding and EHT principle is the use of an irreducible representation of the tight-binding Hamiltonian which is directly fitted to available band structure data without employing explicit basis sets. In EHT, however, one works directly with the orbital basis functions out of which the Hamiltonian elements are constructed using the Hückel principle. The diagonal elements (onsite energies $E_{\mu\mu}$) are benchmarked with experimental values of electronic "hardness," i.e., the difference between ionization potential and electron affinity.[19] The off-diagonal matrix elements are then determined directly from the prescription

$$H_{\mu\mu} = E_{\mu\mu},$$

$$H_{\mu\nu} = \tfrac{1}{2}K_{\mathrm{EHT}}S_{\mu\nu}(H_{\mu\mu} + H_{\nu\nu}), \tag{5}$$

$$S_{\mu\nu} = \int d^3\mathbf{r}\,\phi_\mu^*(\mathbf{r})\phi_\nu(\mathbf{r}),$$

where μ and ν label the atomic orbitals and $S_{\mu\nu}$ is the overlap matrix between the orbital basis function ϕ_μ and ϕ_ν, respectively. K_{EHT} is an additional fitting parameter with a value of 1.75 commonly used for molecules and 2.3 for solids.[19,21] In the case of the planar two-dimensional (2D) graphene sheet a good match is achieved for a value of $K_{\mathrm{EHT}} = 2.8$.[22] One important assumption within EHT is that the hopping matrix elements $H_{\mu\nu}$, $\nu \neq \mu$, depend linearly on the overlap matrix $S_{\mu\nu}$ alone.[19] EHT basis functions are usually Slater-type orbitals (STOs), $\Phi_{nlm} = Nr^{n-1}e^{-\zeta r}Y_{lm}(\Theta,\varphi)$, which have the correct asymptotic form at large distance r (n, l, and m denote, respectively, the principle, azimuthal, and magnetic quantum numbers). The individual orbital wave

functions $|q\rangle$ are then approximated by a linear combination of STOs, with coefficients and exponents $\{c_i, \zeta_i\}$ fitted for the individual basis functions to match band structure data. Since the basis sets are directly fitted to experimental or theoretical data, the resulting AOs are more localized than the free atomic wave functions, although they may still be regarded as long ranged compared to the usual TB Wannier-like description; we typically use a cutoff interatomic distance of R_c=9 Å for the interactions. The use of basis functions that are not too localized turns out to be a key issue for achieving a good transferability.[21] Admittedly, the use of a direction independent K_{EHT} function is a drastic assumption that can be relaxed by making the constant orbital dependent, but we make the simplifying assumption that the orientation dependence arises principally from the corresponding overlap functionals.

The Hückel prescription Eq. (5) can be generalized to connect different chemical subsystems A and B. The problem is that each subsystem has its own parametrization that yields its own vacuum level relative to which electronic levels are calculated. For instance, the Fermi level of most metals is set to E_F=−10 eV in the paper in Ref. 21, which means that each dispersion curve needs to be individually shifted to bring its Fermi level up to the experimental value, through the transformation $\mathbf{H} \rightarrow \mathbf{H} + V_c\mathbf{S}$ for each subsystem. The correct alignment of the levels relative to each other becomes particularly important when studying compound systems such as metal-semiconductor junctions or molecular components attached on nanowires and nanotubes. We calculate the coupling matrix across such a hybrid junction between subsystems A and B using the Hückel principle Eq. (5) through the interpolation scheme

$$\tilde{\mathbf{H}}_{\mu_A\nu_B} = \tfrac{1}{2}\mathbf{S}_{\mu_A\nu_B}[(K_A\mathbf{H}^A_{\mu\mu} + V_{cA}) + (K_B\mathbf{H}^B_{\nu\nu} + V_{cB})], \qquad (6)$$

where V_{cA} and V_{cB} are the shifts needed to align the vacuum levels for subsystems A and B, respectively, and a similar scheme was suggested in Ref. 31. It is worth noting that this approach provides a simple interpolation scheme that gives us the correct limiting values of the Hamiltonian for the two individual subsystems. Further work, however, clearly needs to be done to calibrate this interpolation scheme to specific interfacial properties such as measured charge transfer doping, Schottky barrier heights, or perhaps first-principles calculations of interfacial dipoles or chemisorption properties such as work function modification at surfaces.

IV. RESULTS: NANOTUBE BAND STRUCTURES

We begin by benchmarking our parameters with a two-dimensional graphene sheet. Figure 2 shows the corresponding dispersion relation along the $M \rightarrow \Gamma \rightarrow K \rightarrow M$ path within the 2D Brillouin zone. The dashed line in Fig. 2 is the DFT-GGA calculation of the E-k dispersion, calculated using the SIESTA code,[22,23] to which the EHT band structure is fitted (solid line) by adjusting the onsite Hamiltonian matrix elements H_{ii}, the exponentials, and the expansion coefficients of the Slater-orbital basis functions. As atomiclike basis functions for each carbon atom we are using two basis sets: (i) sp^3 and (ii) sp^3d^5 orbitals, each of which has been optimized to match the DFT-GGA band structure. The two parameter sets are given in Table I. In our calculation all atoms within a cutoff radius of 9 Å from the two nonequivalent atoms within a unit cell are included. Furthermore, we set the Fermi level of graphene to E_F=0.0 eV and K_{EHT} is set to 2.8.[32]

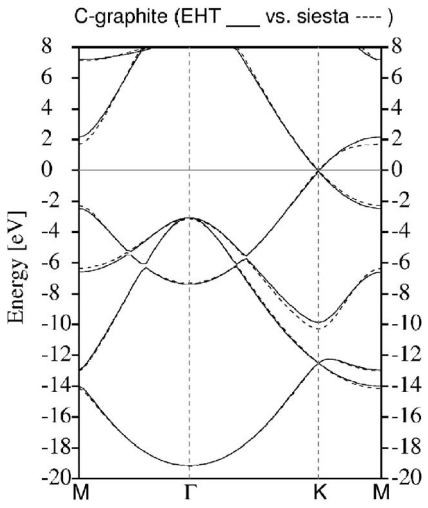

FIG. 2. 2D band structure of a graphene sheet along the $M \rightarrow \Gamma \rightarrow K \rightarrow M$ path within the first Brillouin zone. The solid line corresponds to the EHT band structure using parameters optimized to match the DFT-GGA band structure (dashed line), see Refs. 22 and 23. The C–C bonding distance is set to $a_{\mathrm{C-C}}$=1.44 Å, and the cutoff radius for the neighbor atoms is R_c=9 Å. The Fermi level is at E_F=0.0 eV.

Carbon nanotubes with chirality (n,m) are obtained by wrapping the two dimensional graphene sheet along specific circumference vectors $\mathbf{C}(n,m)=n\mathbf{a}_1+m\mathbf{a}_2$.[33] Note that this approach, being truly atomistic, goes beyond the conventional zone-folding scheme. In the following, we will examine the transferability of the two EHT parameter sets (*sp* and *spd*) of graphene to band structures for small diameter nanotubes. In our calculation, we assume that structural variations of the CNT affect its hopping elements H_{ij} only through the overlap matrix S_{ij} [see Eq. (5)]. This assumption means that the redistribution of charge due to structural changes is discarded, so that the band structure is determined in a non-self-consistent manner. For all tubes considered here, we include the coupling of nearest-neighbor unit cells which consist of two rings each in the case of armchair (n,n) tubes (translation vector T_0=2.39 Å) and four rings for zigzag $(n,0)$ CNTs (T_0=4.32 Å).

TABLE I. EHT parameters for carbon fitted to the 2D band structure of graphene calculated using DFT-GGA (Refs. 22 and 23). For both parameter sets the parameter K_{EHT} was set to 2.8.

	AO	E_{on}	ζ_1	c_1	ζ_2	c_2
C *sp*	2*s*	−20.316	2.037	0.741		
	2*p*	−13.670	1.777	0.640	3.249	0.412
C *spd*	2*s*	−19.889	2.025	0.764		
	2*p*	−13.080	1.624	0.272	2.177	0.739
	3*d*	−2.046	1.194	0.491		

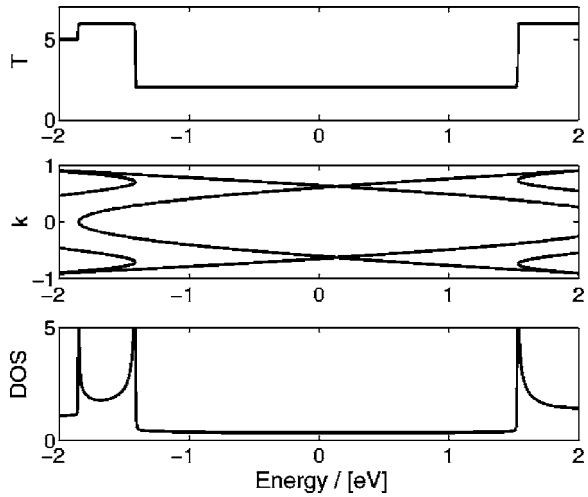

FIG. 3. Band structure, transmission, and DOS per spin for an armchair (5, 5) tube using sp^3 orbitals. Due to their mirror symmetry the curvature of the tube does not break this symmetry, so that the tube remains strictly metallic. The Fermi level is E_F=0.0 eV and k is in units of π/T_0.

A. Metallic armchair tubes

Figure 3 shows the band structure, transmission, and density of states (DOS) for a (5,5) armchair tube within a sp^3-EHT model. The DOS shows typical features of a one-dimensional system, with a constant value within an energy interval of $[-1.5, 1.5]$ eV, and van Hove singularities (VHSs) at the onsets of higher subbands. The transmission per spin within the interval $[-1.5, 1.5]$ eV is 2 indicating that two bands can in principle contribute to transport. Including spin, one should then observe a maximum linear response (zero bias) conductance of $G=2G_0$ with $G_0=2e^2/h$ assuming no parasitic resistances posed by contact interfaces. Notably, curvature effects do not disrupt the band structure of armchair tubes, which stay metallic because the mirror symmetry is not broken upon wrapping the graphene sheet.

B. Curvature effects on nonarmchair "semimetallic" tubes

Experimentally it is known that small diameter carbon nanotubes that are normally expected to be metallic by the $m-n$ rule,[33] with (9,0) and (12,0) chiralities, for example, exhibit a curvature-induced gap than $k_BT \approx 25$ meV (Ref. 34) at the Fermi energy. A simple π-orbital tight-binding model[33–36] commonly employed in CNT transport simulations usually does not account for this effect, but such s-p hybridizations might be important to include when considering CNTs as possible candidates for interconnects. For tubes with diameters $d \leqslant 1$ nm, the structural deformation of the graphene sheet affects its electronic structure significantly enough that such an opening of a band gap can be induced. The opening arises due to a reduction of the overlap between the nearest-neighbor π orbitals under deformation causing the Fermi wave vector k_F to move away from the K point within the first Brillouin zone.[34,37] The more complex sp^3- and the sp^3d^5-EHT models we are using naturally account for these structural deformations (Figs. 4 and 5) through the structure-dependent overlap matrix **S**, see Eq. (5), yielding

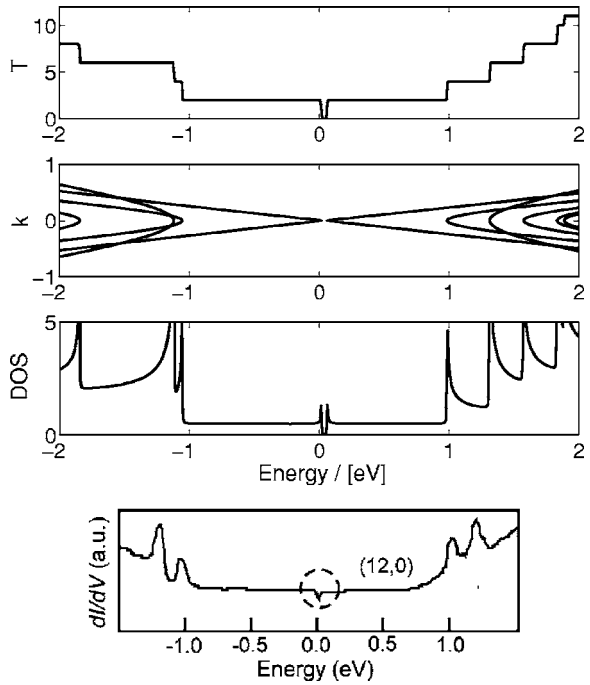

FIG. 4. Band structure, DOS, and transmission per spin for a "metallic" zigzag (12, 0) tube using sp^3 orbitals. The gap close to the Fermi level at E_F=0.0 eV is about 50 meV. For comparison the experimental STS-dI/dV signal is shown at the bottom (Ref. 34). The bottom figure has been reprinted with permission from Ref. 34. Copyright 2001 American Association for the Advancement of Science.

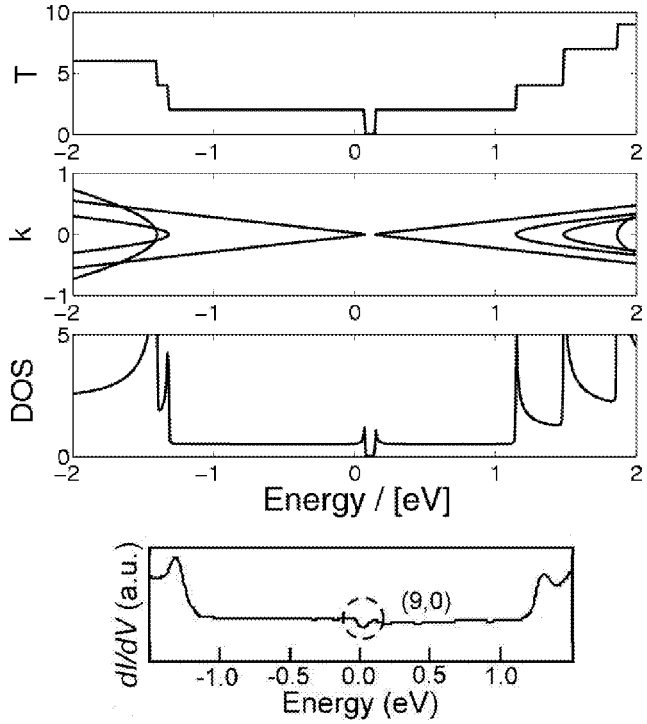

FIG. 5. Band structure, DOS, and transmission per spin for a "metallic" zigzag (9, 0) tube using sp^3 orbitals. The gap close to the Fermi level at E_F=0.0 eV is about 80 meV similar to STS-dI/dV measurements as shown at the bottom (Ref. 34). The bottom figure has been reprinted with permission from Ref. 34. Copyright 2001 American Association for the Advancement of Science.

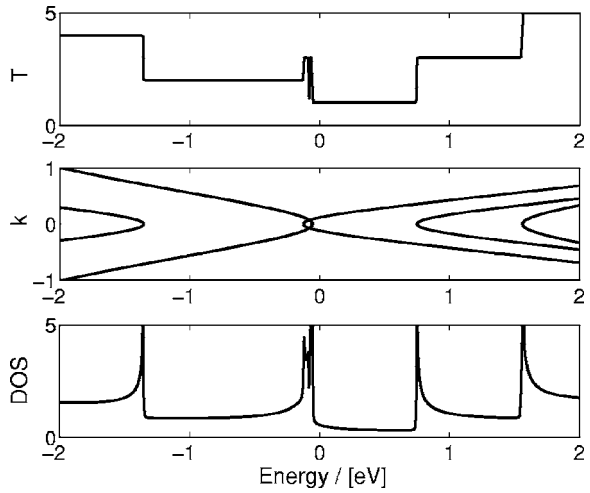

FIG. 6. Band structure, DOS, and transmission per spin for a zigzag (5, 0) tube using sp^3 orbitals. Due to the crossing of the bands around $E_F \approx 0.0$ eV, the tube becomes metallic.

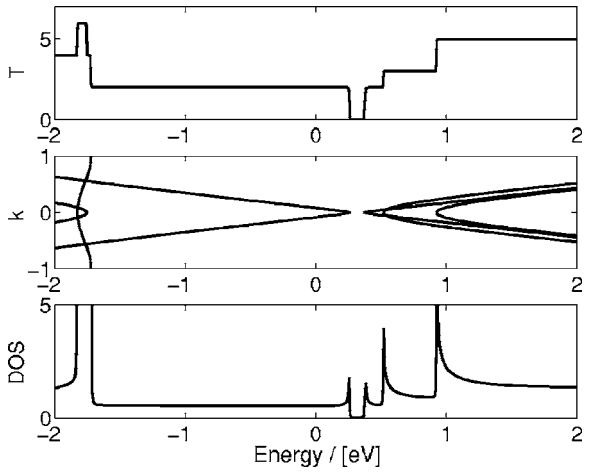

FIG. 7. Band structure, DOS, and transmission per spin for a zigzag (6, 0) tube using sp^3 orbitals. The "metallic" tube becomes semiconducting with a band gap of ≈ 0.1 eV and shift of the Fermi level from 0.0 to ≈ 0.3 eV.

for our bulk graphene parameters a gap that actually compares quite well quantitatively in the case of a sp^3 model with experimental scanning tunneling spectra (see Table II), whereas our sp^3d^5 model shows a poorer quantitative match for these class of tubes.

C. Ultrasmall diameter tubes

For ultrasmall nanotube diameters, hybridization effects start to become dominant. Figure 6 shows that the (5,0) zigzag tube, semiconducting in a zone-folding method, is predicted by EHT to become metallic for the case of a *sp*-orbital model, since the valence and conduction bands cross at $E_F \approx 0.0$ eV. On the other hand, the zigzag (6,0) tube moves the other way (Fig. 7), from being metallic in a zone-folding method to semiconducting in EHT with a band gap of ≈ 0.12 eV due to strong hybridization effects. DFT-GGA calculations, however, show that a (6,0) tube remains metallic due to rehybridization.[38,39] Using in turn *spd* orbitals for carbon, our EHT model agrees with the DFT-GGA results for these small diameter tubes. While the accuracy of DFT for semiconducting band gaps is itself open to question, the contradictory result for the *sp*-orbital model could also imply that the inclusion of deformation effects through just the off-diagonal EHT Hamiltonian elements is no longer a valid assumption and the onsite energies themselves need to be recalculated self-consistently to include the effect of the electrostatics on the local atomic potentials.

For large deformations, a fully self-consistent calculation of the band structure might be necessary to describe the electronic structure properly. If the tube has a large curvature, the respective charge distributions inside and outside the tube become asymmetric[38] leading to the formation of dipoles. Due to the charge redistribution and the dipolar electric fields, the individual bands are shifted such that the (6,0) tube remains metallic in DFT-GGA. The processes of charge redistribution, dipole formation, and the floating of the bands, however, require a fully self-consistent band structure calculation that can be set up within the Poisson NEGF approach[16] but have not yet been incorporated within our present computational scheme. Note that this is not a shortcoming of the extended Hückel theory itself but arises instead from the importance of self-consistent electrostatic effects that have been discarded for simplicity in the band structure calculation. Table II compares the band gaps for the studied tubes both with respect to STS experiments as well as other theoretical calculations. Our results based on extended Hückel theory are in good agreement with more sophisticated DFT approaches and experiments, in fact, local density approximation (LDA) suffers from the well-known band gap problem that an EHT approach calibrated to graphene seems to bypass. This suggests that an EHT scheme, supplemented by self-consistent electrostatics, might be a good compromise between simple π-orbital tight-binding theories and computationally expensive DFT methods, the practicality of the scheme being particularly important when modeling transport through large complex nanostructures.

V. NANOTUBES AS CHEMICAL SENSORS

While the previous examples test our EHT prescription for band structure calculations of bare CNTs, we now combine it with molecule chemistry. It has been suggested that the chemisorption of CO molecules could be enhanced by deforming the CNT, so that the regions of highest curvature have an enhanced chemical reactivity.[40] Based on a first-principles calculation within GGA, da Silva *et al.* have shown that a semiconducting (8,0) CNT can become metallic upon lateral deformation to an elliptical shape, but thereafter the semiconducting state can be recovered by attaching a CO molecule at the spot of highest curvature.[24] This seems to indicate that highly deformed CNTs are possible candidates for sensing CO molecules by means of a band gap variation and corresponding metal-insulator transition. We use the DFT calculations by da Silva *et al.* as a qualitative benchmark to explore the accuracy of EHT for electronic structure in the presence of a periodic array of CO molecules, of which one unit cell is shown in Fig. 8.

TABLE II. Comparison of experimentally and theoretically determined band gaps (in units of eV) using different theoretical methods. TB denotes orthogonal tight binding, CNT bands refer to a simple π-orbital description with one hopping parameter γ, DFT is density functional theory using different approximations for exchange-correlation potential, and EHT with *sp* or *spd* orbitals for carbon (Ref. 22).

(n,m)	TB	CNT bands	DFT	Expt.	EHT *sp*	EHT *spd*
(5,0)	⋯	1.91 (γ=2.5) 2.29 (γ=3.0)	0.0[a]	⋯	−0.05	0.0
(6,0)	0.05[b] ~0.2[c] 0.179[d]	0.0	−0.83[b] 0.0[a]	⋯	0.12	0.0
(9,0)	0.2[a] 0.075[d] 0.07[b] ~0.04[c]	0.0	0.2[a] (GGA) 0.17[b] (LDA) 0.12[f] (LDA) 0.17[f] (GW)	0.080±0.005[e]	0.075	0.13
(10,0)	0.65[g] 0.87[g] 0.85[c]	0.91 (γ=2.5) 1.09 (γ=3.0)	0.88[a] (GGA) 0.8[i] (GGA)	0.83[h]	0.91	0.95
(12,0)	0.08[a] 0.0[c]	0.0	0.08[a] (GGA) 0.057[j] (LDA)	0.042±0.004[e]	0.045	0.077
(13,0)	~0.7[c]	0.70 (γ=2.5) 0.84 (γ=3.0)	0.73[a] (GGA)	⋯	0.71	0.74
(15,0)	0.0[c]	0.0	0.14[a] (GGA) 0.038[j] (LDA)	0.029±0.004[e]	0.026	0.05
(16,0)	⋯	0.56 (γ=2.5) 0.68 (γ=3.0)	0.61[a] (GGA)	0.65±0.30[k]	0.59	0.6

[a]Reference 39.
[b]Reference 38.
[c]Reference 42.
[d]Reference 43.
[e]Reference 34.
[f]Reference 44.
[g]Reference 45.
[h]Reference 46.
[i]Reference 47.
[j]Reference 48.
[k]Reference 49.

Our starting point is the band structure of an undeformed semiconducting (8,0) tube using *spd*-EHT parameters optimized for 2D graphene with the Fermi level set at $E_F=-13$ eV.[22] The transferability of the *sp*-as well as the *spd*-orbital EHT parameters has been discussed in the previous section. Setting our vacuum level as the zero energy reference, we shift the CNT Fermi energy by $V_c=+8.5$ eV towards the experimental Fermi level of 2D graphene, i.e., $E_F=-4.5$ eV, employing the modified Hückel prescription, see Eq. (6). Following Ref. 24 we deform the tube perpendicular to its axis so that the minor axis is 30% of the original tube radius of $R_t=6.3$ Å, cf. Fig. 8.

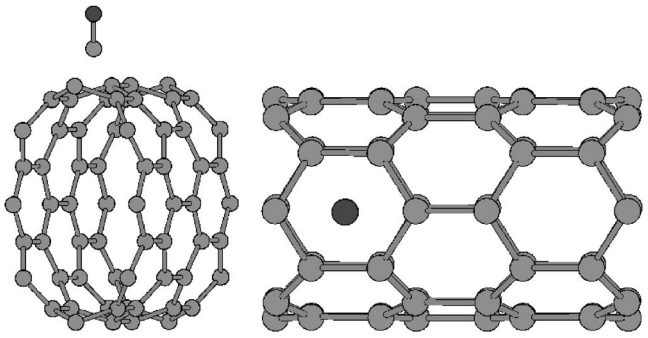

FIG. 8. Unit cell of a semiconducting (8, 0) CNT with one CO molecule at distance of $d=1.85$ Å from the CNT surface. The CO molecule has been placed above the center of the hexagon which is the most stable equilibrium position after relaxation (Ref. 24). The unit cell of the periodic structure consist of two (8, 0) CNT unit cells and one CO molecule, i.e., the cell contains 66 atoms.

To ensure that our strongly deformed structure really corresponds to the local minimum of the total energy, we optimize the deformed tube unit cell by means of GAUSSIAN 03 (Ref. 41) using the spin unrestricted LDA approach within the Slater-Vosko-Wilk-Nusair (SVWN) approximation. During the optimization we froze two row atoms along the opposite extremes of the minor axis, while edge effects were eliminated from the optimized structure by employing periodic boundary conditions within GAUSSIAN 03 for structure optimization, with a translation vector of 4.32 Å along the tube axis. We note that compared to that of da Silva *et al.*[24] our system being optimized consists of only one unit cell of a (8,0) tube instead of two.

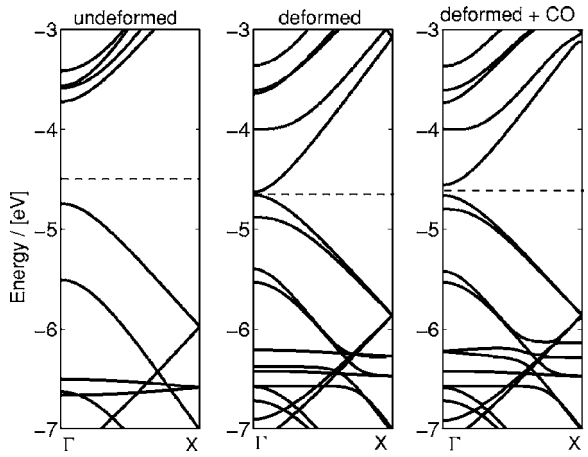

FIG. 9. Band structures of a zigzag (8, 0) CNT using sp^3d^5 orbitals. Left: undeformed tube with a band gap of $E_G \approx 1.1$ eV, middle: deformed tube with a small gap of $E_G \approx 25$ meV, and right: deformed tube with attached CO molecule at distance 1.85 Å. The gap here is $E_G \approx 100$ meV. The Fermi energy is indicated by the dashed line.

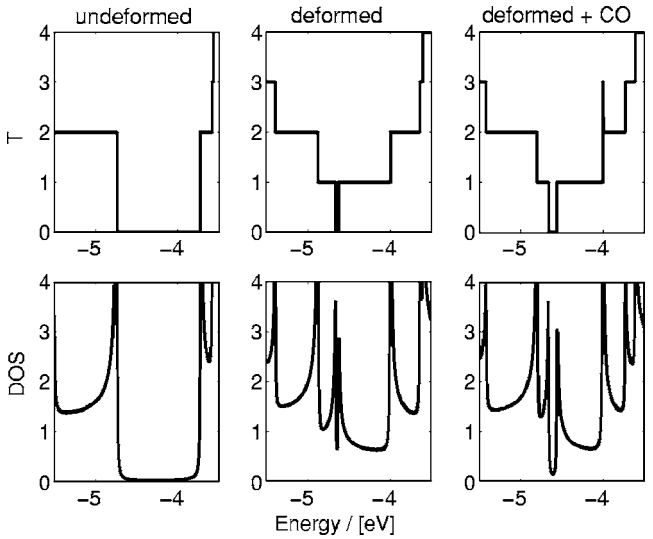

FIG. 10. DOS and transmission per spin for the semiconducting (8, 0) CNT. Left: undefomed, middle: deformed, and right: deformed with attached CO molecule.

Since the EHT levels are correct up to an overall shift, we start by aligning the levels of the CO molecule and the CNT. The highest occupied molecular orbital (HOMO) of CO, calculated within GAUSSIAN 03 using the Becke 3 parameter exchange with Perdew-Wang 91 correlation (B3PW91) with 6-31G(d) basis sets is $E_H = -10.14$ eV relative to vacuum. The corresponding value in our EHT parametrization is $E_H = -14.09$ eV, so that we need an overall shift $V_{c,\mathrm{CO}} = +3.95$ eV. After this shift is executed, the CO molecule is attached to the tube at the point where its curvature is highest. According to Ref. 24 the most favorable location to place the CO molecule is above the center of a hexagon, as shown in Fig. 8. Since we are only interested in the effect of one single CO molecule on the tube dispersion, we need to avoid any overlap between neighboring CO molecules. This is accomplished by using two CNT (8,0) unit cells and attaching only one CO molecule. The effective periodicity of the system is then 8.64 Å, large enough that the neighboring CO molecular basis functions do not overlap.

Figure 9 shows the dispersion and Fig. 10 the respective DOS and transmission per spin for the combined CNT-molecular system. The original band gap $E_G = 1.1$ eV of the undeformed tube (left) shrinks down to $E_G \approx 30$ meV upon the 30% lateral deformation, so that the tube becomes effectively metallic at room temperature (center). Attachment of the CO molecule on the deformed CNT (right) makes the tube semiconducting once again, with a band gap of $E_G \approx 100$ meV, much less than that of the undeformed tube, but noticeably larger than thermal energies at room temperature. Our results agree qualitatively with those of da Silva and co-workers,[24,40] even though there are quantitative differences: the initial band gap of the undeformed tube is 0.66 eV and becomes completely closed after lateral deformation, so that the tube becomes truly metallic. The recovered band gap upon CO attachment is with ≈200 meV, of similar order as in our case with 100 meV. The largest source of disagreement is the band gap of the undeformed CNT; given that DFT-LDA/GGA calculations used to underestimate band gaps (see Table II) and are hence often questionable, a quantitative resolution of this discrepancy may need experimental attention.

Note that the present calculations are all non-self-consistent, ignoring effects due to the rearrangement of charges during tube deformation, as well as those arising from charge transfer between the molecular species and the nanotube, while a proper self-consistent calculation as discussed in the last section is needed to do quantitative justice to this problem. Nonetheless, the EHT parameters seem to be quite transferable between band structure as well as surface chemistry, in particular for strongly deformed structures without the need for any reparametrization. This makes EHT a good compromise between accuracy and practicality. In our follow-up paper,[25] we will demonstrate the applicability of EHT to modeling silicon, including its transferability between bulk and multiple surface band structures of reconstructed silicon surfaces and also for nanowires. Applying this approach has allowed us to quantitatively explain and in some cases even predict interesting experimental results involving molecular conductors on silicon.[1,2]

VI. FUTURE WORK

For transport calculations, we often need a minimal model that can do justice to band structure, electrostatic, as well as bonding chemistry. This becomes particularly important if one wants to deal with strongly deformed structures, interfaces, or combinations thereof including molecules. We have shown that extended Hückel theory provides a good practical compromise to capture various aspects of band structure and chemistry. The two attributes that make this semiempirical approach especially useful are the presence of explicit basis sets and nonorthogonality. To make this chemists' approach to band structure of further use, it may be preferable to work with a self-consistent *complete neglect of differential overlap* (CNDO) approach to bring in differential Coulomb costs into the picture.

For many nanoscale structures such as nanotubes and nanowires, perhaps even interfacing with smaller molecules, we believe that a semiempirical approach combining band structure and chemistry is essential, given that typical tight-binding theories are not transferable beyond small deformations while DFT theories are computationally quite prohibitive. The latter becomes even more difficult to implement when we want to move from equilibrium electronic structure to more complicated nonequilibrium transport problems. It is generally acknowledged that much of the conducting properties of nanostructures are dominated by their interfaces and contacts. It is in this complicated domain that we believe the real strength of a nonorthogonal theory with explicit basis sets such as EHT or CNDO is likely to manifest itself.

ACKNOWLEDGMENTS

The authors acknowledge the support of the Army Research Office through the Defense University Research Initiative in Nanotechnology (DURINT) program, the Army Research Office (ARO), and the Network for Computational Nanotechnology (NCN). One of the authors (J.I.C.) acknowledges support from the Spanish DGICyT and CAM under Contract Nos. MAT2004-05348-C04-2 and MAT/0440/2004, respectively. The authors are indebted to M. P. Anantram and M. S. Lundstrom for helpful discussions.

[1]T. Rakshit, G. C. Liang, A. W. Ghosh, and S. Datta, Nano Lett. **4**, 1803 (2004).
[2]G. C. Liang and A. W. Ghosh, Phys. Rev. Lett. **95**, 076403 (2005).
[3]J. Park *et al.*, Nature (London) **417**, 722 (2002).
[4]B. Muralidharan, A. W. Ghosh, and S. Datta, Phys. Rev. B **73**, 155410 (2006)
[5]C. M. Goringe, D. R. Bowler, and E. Hernandez, Rep. Prog. Phys. **60**, 1447 (1997).
[6]A. Peccia and A. Di Carlo, Rep. Prog. Phys. **67**, 1497 (2004).
[7]D. Kienle and A. W. Ghosh, J. Comput. Electron. **4**, 97 (2005).
[8]P. Vogl, H. P. Hjalmarson, and J. D. Dow, J. Phys. Chem. Solids **44**, 365 (1983).
[9]J.-M. Jancu, R. Scholz, F. Beltram, and F. Bassani, Phys. Rev. B **57**, 6493 (1998).
[10]T. Boykin, G. Klimeck, and F. Oyafuso, Phys. Rev. B **69**, 115201 (2004).
[11]P. N. Keating, Phys. Rev. **145**, 637 (1966).
[12]R. G. Parr and W. Yang, *Density-Functional Theory of Atoms and Molecules* (Cambridge University Press, New York, 1994).
[13]U. von Barth, Phys. Scr., T **T109**, 9 (2004).
[14]R. M. Martin, *Electronic Structure: Basic Theory and Practical Methods* (Cambridge University Press, New York, 1994).
[15]J. Taylor, H. Guo, and J. Wang, Phys. Rev. B **63**, 245407 (2001).
[16]P. S. Damle, A. W. Ghosh, and S. Datta, Phys. Rev. B **64**, 201403 (2001).
[17]M. Brandbyge, J.-L. Mozos, P. Ordejon, J. Taylor, and K. Stokbro, Phys. Rev. B **65**, 165401 (2002).
[18]N. Sai, M. Zwolak, G. Vignale, and M. Di Ventra, Phys. Rev. Lett. **94**, 186810 (2005)
[19]J. N. Murrell and A. J. Harget, *Semi-empirical Self-consistent-field Molecular Orbital Theory of Molecules* (Wiley-Interscience, New York, 1972).
[20]W. Tian, S. Datta, S. Hong, R. Reifenberger, J. Henderson, and C. P. Kubiak, J. Chem. Phys. **109**, 2874 (1998).
[21]J. Cerda and F. Soria, Phys. Rev. B **61**, 7965 (2000).
[22]http://www.icmm.csic.es/jcerda/index.html
[23]J. M. Soler, E. Artacho, J. D. Gale, A. Garcia, J. Junquera, P. Ordejon, and D. Sanchez-Portal, J. Phys.: Condens. Matter **14**, 2745 (2002).
[24]L. B. da Silva, S. B. Fagan, and R. Mota, Nano Lett. **4**, 65 (2004).
[25]D. Kienle, K. H. Bevan, G.-C. Liang, L. Siddiqui, J. I. Cerda, and A. W. Ghosh, J. Appl. Phys. **100**, 043715 (2006), following paper.
[26]H. Haug and A. P. Jauho, *Quantum Kinetics in Transport and Optics of Semiconductors* (Springer, Berlin, 1996).
[27]S. Datta, *Electronic Transport In Mesoscopic Systems* (Cambridge University Press, New York, 1995).
[28]M. P. L. Sancho, J. M. L. Sancho, and J. Rubio, J. Phys. F: Met. Phys. **14**, 1205 (1984).
[29]M. P. L. Sancho, J. M. L. Sancho, and J. Rubio, J. Phys. F: Met. Phys. **15**, 851 (1985).
[30]J. C. Slater and G. F. Koster, Phys. Rev. **94**, 1498 (1954).
[31]G. Kirczenow, P. G. Piva, and R. A. Wolkow, Phys. Rev. B **72**, 245306 (2005).
[32]Note that in the EHT parameter optimization, the Fermi level for graphene is set to $E_F=-13$ eV, so that the bands are unique up to an overall shift (Refs. 21 and 22). The role of the Fermi energy in parameter fitting has been addressed in Sec. III. Its absolute value, however, becomes particularly important for compound systems as shown in Sec. V.
[33]R. Saito, G. Dresselhaus, and M. S. Dresselhaus, *Physical Properties of Carbon Nanotubes* (Imperial College Press, London, 2003).
[34]T. W. Odom, M. Ouyang, J. L. Huang, C. L. Cheung, and C. M. Lieber, Science **292**, 702 (2001).
[35]F. Triozon, P. Lambin, and S. Roche, Nanotechnology **16**, 230 (2005).
[36]H. Liu and Y. Tao, Nanotechnology **16**, 619 (2005).
[37]L. Yang and J. Han, Phys. Rev. Lett. **85**, 154 (2000).
[38]X. Blase, L. X. Benedict, E. L. Shirley, and S. G. Louie, Phys. Rev. Lett. **72**, 1878 (1994).
[39]G. Sun, J. Kürti, M. Kertesz, and R. H. Baughman, J. Phys. Chem. B **107**, 6924 (2003).
[40]S. B. Fagan, L. B. da Silva, and R. Mota, Nano Lett. **3**, 289 (2003).
[41]M. J. Frisch *et al.*, GAUSSIAN 03, Revision C.02, Gaussian, Inc., Wallingford, CT, 2004.
[42]N. Hamada, S. Sawada, and A. Oshiyama, Phys. Rev. Lett. **68**, 1579 (1992).
[43]J. X. Cao, X. H. Jan, J. W. Ding, and D. L. Wang, J. Phys.: Condens. Matter **13**, L271 (2001).
[44]T. Miyake and S. Saito, Phys. Rev. Lett. **72**, 073404 (2005).
[45]H. Yorikawa and S. Muramatsu, Phys. Rev. B **52**, 2723 (1995).
[46]T. W. Odom, J. L. Huang, P. Kim, and C. M. Lieber, J. Phys. Chem. B **104**, 2794 (2000); note that since the value for the (8, 0), CNT is not given explicitly, we have determined its band gap from the STS plot by measuring the distance between the first VHS where the STS is negligible, so that a gap can be clearly identified. The distance between the largely broadenend peaks is about 1.1 eV.
[47]P. V. Avramov, K. N. Kudin, and G. E. Scuseria, Chem. Phys. Lett. **370**, 597 (2003).
[48]T. Miyake (private communication), the band gaps for the (12, 0), and (15, 0), CNTs are based on LDA calculations.
[49]J. W. G. Wildboer, L. C. Venema, A. G. Rinzler, R. E. Smalley, and C. Dekker, Nature (London) **391**, 59 (1998).